of Earth and Venus are quantitatively similar, even though the terrestrial and venusian atmospheric compositions are quite different. Although the green line intensity is potentially a measure of oxygen atom densities in planetary atmospheres, the present measurement demonstrates that green line production is not limited to planets with an Earth-like atmosphere.

The high venusian green/red line intensity ratio leads to the conclusion that the green line originates in the atom recombination region, rather than in the ionosphere. Ionospheric production strongly favors the red line, and Fox (*22*) predicts 46 R of red line emission from the Venus ionosphere but only 1 to 2 R of green line. Because the venusian atomic oxygen 630-nm red line intensity is no more than 10 to 15% that of the green line, we conclude that the $O(^1S)$ is being produced via Eqs. 1 and 2 near 100-km altitude, not via Eq. 3.

The identity of the O_2^* intermediate is controversial (*23*, *24*), although in recent years $O_2(c)$ has been favored (*25*), although among the three Herzberg states generated in the terrestrial atmosphere $O_2(c)$ emission is the weakest (*5*, *6*). In the venusian atmosphere, the situation is reversed and the $O_2(c)$ emission is the strongest (*4*), but the single vibrational level observed has insufficient energy to generate the green line by Eq. 2. Since the Venera missions, these two facts appeared to support each other. Now the mechanisms must be reconsidered.

The other O_2 emitter identified in the Venus visible spectrum thus far, the v = 0 level of the $O_2(A')$ state (*12*), has 0.08 eV more energy than needed to generate the green line via Eq. 2. The total intensity of its v′ = 0 progression (based on 120 R in the Chamberlain 0-6 band) is 700 R, i.e., somewhat more than all the emission from the Herzberg states in the terrestrial atmosphere (*5*, *6*). We also note that if venusian emission from $O_2(c, v \geq 2)$, suspected of being the transfer agent in the terrestrial atmosphere, had the same intensity as on Earth [about 100 R (*5*)] it would be indiscernible in the Keck/HIRES or the Venera spectra because it would be spread among many bands and rotational levels.

Lastly, it is important to point out that despite the O_2 Herzberg II band emission and the far more intense O_2 Infrared Atmospheric band emission at 1.27 μm (*8*), ground-state O_2 is reactively destroyed in the Venus environment (*26*). Absorption measurements using scattered solar light from the dayside reveal an upper limit on the O_2 mixing ratio between 10^{-6} and 10^{-7} (*27*).

References and Notes

1. J. L. Fox, *Can. J. Phys.* **64**, 1631 (1986).
2. ———, in *Venus and Mars: Atmospheres, Ionospheres, and Solar Wind Interactions, Geophys. Monogr. Am. Geophys. Union 66*, J. G. Luhmann, M. Tatrallyay, R. O. Pepin, Eds., Geophysical Monographs 66 (American Geophysical Union, Washington, DC, 1992), pp. 191–222.
3. ———, in *Atomic, Molecular, and Optical Physics Handbook*, G. W. F. Drake, Ed. (AIP Press, Woodbury, NY, 1996), pp. 940–968.
4. V. A. Krasnopolsky, A. A. Krysko, V. N. Rogachev, V. A. Parshev, *Cosmic Res.* **14**, 789 (1976).
5. T. G. Slanger, D. L. Huestis, *J. Geophys. Res.* **86**, 3551 (1981).
6. J. Stegman, D. P. Murtagh, *Planet. Space Sci.* **39**, 595 (1991).
7. The terrestrial green line intensity is rather high for the tropical nightglow (*28*), but because the measurements were made only 20 min before sunrise there is a large dayglow component. The solar depression angle of only 5° corresponds to a shadow height of 25 km, so the ionosphere is well illuminated and both the green and red lines are strong, with an intensity ratio I(630)/I(557.7) of about 3. In the nightglow, this ratio is considerably less than unity, approaching zero as the ionospherically produced $O(^1D)$ decays away, whereas the $O(^1S)$ concentration only falls to the level determined by its generation in the ~95-km atom recombination region.
8. D. Crisp *et al.*, *J. Geophys. Res.* **101**, 4577 (1996).
9. There have been no high-resolution determinations of the term energy of the $O_2(c, v = 0)$ level, so we rely on calculations reported in (*29*), which are based on experimental data for v ≥ 1 (*30*), to calculate the line positions. We find that 0.71 cm^{-1} must be added to the calculated v = 0 term energy to conform to the Keck-Venus data, which now become the standard for the $O_2(c, v = 0)$ level position.
10. D. R. Bates, *Planet. Space Sci.* **37**, 881 (1989).
11. G. M. Lawrence, C. A. Barth, V. Argabright, *Science* **195**, 573 (1977).
12. T. G. Slanger, G. Black, *Geophys. Res. Lett.* **5**, 947 (1978).
13. P. Connes, J. F. Noxon, W. A. Traub, N. P. Carleton, *Astrophys. J.* **233**, L29 (1979).
14. A. I. Stewart, D. E. Anderson Jr., L. W. Esposito, C. A. Barth, *Science* **203**, 777 (1979).
15. P. D. Feldman, H. W. Moos, J. T. Clarke, A. L. Lane, *Nature* **279**, 221 (1979).
16. A. I. Stewart, C. A. Barth, *Science* **205**, 59 (1979).
17. D. L. Huestis, T. G. Slanger, *J. Geophys. Res.* **98**, 10,839 (1993).
18. S. W. Bougher, W. J. Borucki, *J. Geophys. Res.* **99**, 3759 (1994).
19. V. A. Krasnopolsky, *Planet. Space Sci.* **29**, 925 (1981).
20. ———, *Planet. Space Sci.* **34**, 511 (1986).
21. S. Akasofu, *Eos* **80**, 397 (1999).
22. J. L. Fox, *Adv. Space. Res.* **10**, 31 (1990).
23. S. Chapman, *Proc. R. Soc. London* **132**, 353 (1931).
24. C. A. Barth, *Science* **134**, 1426 (1961).
25. D. R. Bates, *Planet. Space Sci.* **36**, 883 (1988).
26. G. A. Rowland, L. F. Phillips, *Geophys. Res. Lett.* **27**, 3301 (2000).
27. J. T. Trauger, J. I. Lunine, *Icarus* **55**, 272 (1983).
28. S. P. Zhang, G. G. Shepherd, *Geophys. Res. Lett.* **26**, 529 (1999).
29. T. G. Slanger, P. C. Cosby, *J. Phys. Chem.* **92**, 267 (1988).
30. D. A. Ramsay, *Can. J. Phys.* **64**, 717 (1986).

31. This report is based on observations made at the W. M. Keck I telescope, which is operated jointly by the California Institute of Technology and the University of California. Supported by the NASA Planetary Astronomy program.

26 September 2000; accepted 22 November 2000

Birth of the Kaapvaal Tectosphere 3.08 Billion Years Ago

D. E. Moser,[1*] R. M. Flowers,[1†] R. J. Hart,[2]

The crustal remnants of Earth's Archean continents have been shielded from mantle convection by thick roots of ancient mantle lithosphere. The precise time of crust-root coupling (tectosphere birth) is poorly known but is needed to test competing theories of continental plate genesis. Our mapping and geochronology of an impact-generated section through the Mesoarchean crust of the Kaapvaal craton indicates tectosphere birth at 3.08 ± 0.01 billion years ago, roughly 0.12 billion years after crust assembly. Growth of the southern African mantle root by subduction processes occurred within about 0.2 billion years. The assembly of crust before mantle may be common to the tectosphere.

As one of Earth's oldest surviving fragments of continental lithosphere, the Kaapvaal craton is a valuable archive for understanding the processes that generated the Archean continents. The crystallization ages of the Kaapvaal crust range from 3.6 to 2.6 billion years ago (Ga) [(*1*) and references therein] and its mantle root is as old as 3.5 billion years (Gy) (*2*); however, the time at which the crust and mantle became physically coupled to form a thick (150 to 300 km), stable continental plate [i.e., tectosphere (*3*)] is poorly known. At issue for all tectosphere is whether the conjoined mantle root and crust formed together (*4*) or separately (*3*, *5*). The age of Kaapvaal tectosphere formation was estimated to be at least 3.3 ± 0.2 Ga, based on Sm-Nd ages from mineral inclusions in diamond (*6*) and on evidence for crustal assembly of its Mesoarchean nucleus by 3.2 Ga (*7*). A craton-wide overprinting episode of granitoid magmatism at 3.1 Ga was attributed to "intracrustal melting" after a 3.2 Ga orog-

[1]Geology and Geophysics Department, University of Utah, 135S 1460E, Salt Lake City, UT 84112–0111, USA. [2]Schonland Research Centre, University of the Witwatersrand, Johannesburg, South Africa.

*To whom correspondence should be addressed. E-mail: demoser@mines.utah.edu

†Present address: Department of Earth, Atmospheric and Planetary Sciences, Massachusetts Institute of Technology, Boston, MA 02139, USA.

eny (*7*), whereas a reported 2.8 Ga thrusting and metamorphic event in the deep crust implied even younger structural and thermal remobilization of the lithosphere (*8*).

We dated the birth of the Kaapvaal tectosphere by determining the last high-temperature metamorphic event to melt and metamorphose the deep crust, assuming this to herald stabilization of and thermal shielding by (*9*) the refractory (*4*) mantle root. We conducted our study on the Vredefort section; a unique, impact-generated exposure of the crust-mantle transition near the center of the craton (*10*) (Fig. 1). A 2.020 ± 0.003 Ga (*11*) meteorite impact pierced the ~10-km-thick sedimentary and volcanic rocks of the 3.07 to 2.5 Ga Witwatersrand Basin (*1*), forming a 300-km diameter impact crater (*12*). Isostatic recovery in the center of the Vredefort impact structure overturned and exposed the lower basin strata and underlying crystalline basement, the latter to paleodepths of at least 20 km (*13*). Recent discovery of 3.5 to 3.3 Ga mantle rocks at the center of the basement uplift further supports the interpretation that the 37-km-thick crust has been turned on edge (*10*).

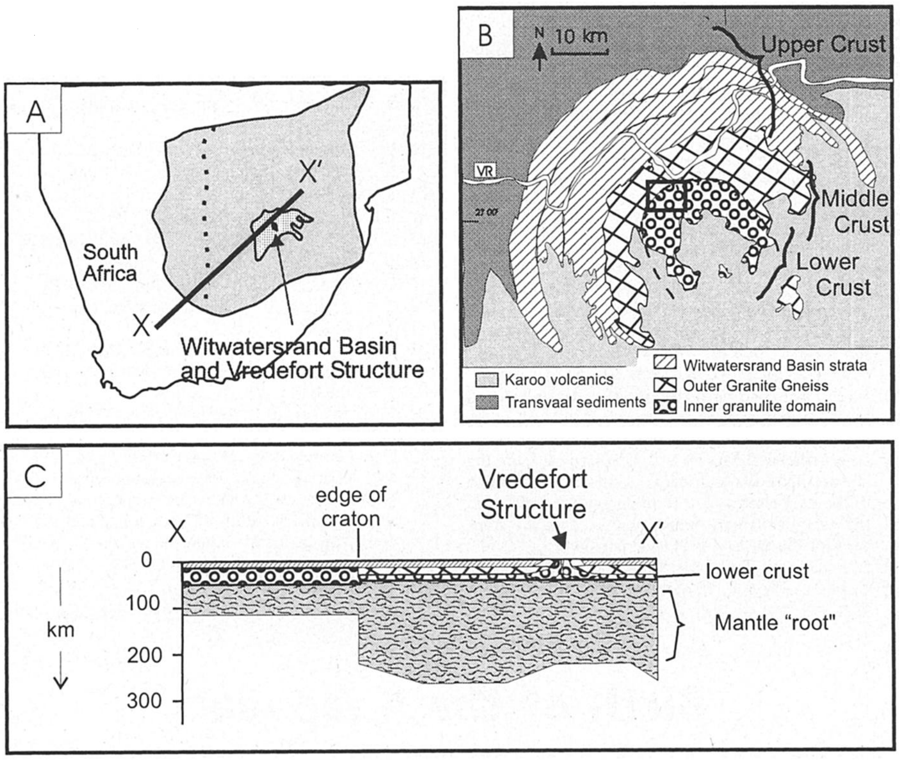

Fig. 1. (**A**) Location of Vredefort impact structure (arrow) near the center of the Kaapvaal craton. Dotted line separates western Neoarchean crust from the Mesoarchean craton core. X-X′ indicates the location of the cross section shown in (C). (**B**) Generalized basement geology map of the core of the Vredefort impact structure showing middle and lower crustal domains. VR, Vaal River. Note location of Fig. 2 (black box) in NW quadrant. (**C**) Interpreted geologic cross section of Kaapvaal lithosphere and Vredefort impact structure, modified from (*7*).

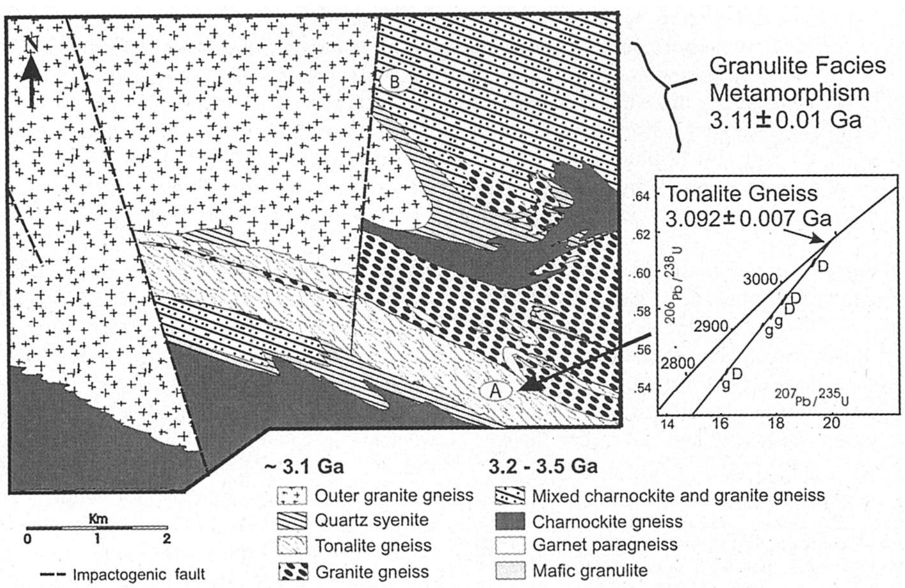

Fig. 2. Detailed map of basement geology across the middle-lower crustal contact within the core of the Vredefort structure. Geochronology sample sites A and B are shown. The concordia plot shows zircon results for the tonalite dyke (D) and gneiss (g). Note the unit of garnet paragneiss, north of site A, which yielded a 3.11 ± 0.01 Ga U-Pb age for metamorphism (*16*).

The middle crustal layer of the Vredefort section, the 10-km-thick outer granite gneiss domain (*14*), is composed mainly of massive to foliated 3.05 ± 0.05 Ga K-feldspar megacrystic granodiorite metamorphosed in the amphibolite facies (*15*). The lower crustal component is a gneiss complex consisting of interlayered felsic gneiss, felsic charnockite, mafic granulite, paragneiss, and sedimentary rocks that yield whole rock Rb-Sr and Th-Pb ages of 3.5 ± 0.2 Ga (*15*) and >3.43 ± 0.03 Ga detrital zircon ages (*16*). An age of 3.11 ± 0.01 Ga for granulite facies metamorphism of the lower crust has recently been determined by dating monazite and zircon in garnetiferous paragneiss and mafic granulites, respectively (*16*). Using high-resolution (1:13,600) airphotos and handheld Global Positioning System receiver units (±4-m accuracy), we generated a geologic map (Fig. 2) to characterize the final stages of Archean deep crustal evolution.

Mapping of the deep crust focused on a 8 km by 7 km area of the best exposures, found in the northwestern quadrant of the central uplift, of the contact between the middle and lower crustal domains (Fig. 2). Our mapping revealed a series of northerly trending impactogenic brittle faults bounding large undisturbed blocks that preserve the pre-impact configuration of the middle and lower crust (*17*) (Fig. 2). In such undisturbed areas, the contact between the middle crust and the lower crust is intrusive and, although subsequently deformed, is transitional over a distance of several kilometers. Tabular, kilometer-scale bodies of quartz syenite in this zone, and spatially associated units of granitic and tonalitic gneiss, cross-cut charnockitic and granulite bodies suggesting a younger (i.e., <3.11 ± 0.01 Ga) component within the lower crustal domain. This age relation is corroborated by our U-Pb zircon geochronology data within this zone.

We determined the primary ages of shock-metamorphosed zircon grains from two sites

(Fig. 2) using techniques described elsewhere (*16*) (Table 1). Site A is situated in the lower crustal granulite complex approximately 6 km beneath the middle crustal granites and consists of deformed fine- to medium-grained tonalite gneiss and cross-cutting 5- to 50-cm-wide dikes of foliated tonalite. A dike sample yielded 4 zircon grains that define a discordia line with upper and lower intercepts of 3.092 ± 0.007 Ga and 2.039 ± 0.049 Ga, respectively, with a probability of fit of 63% (*18*). Zircon data for the gneiss are more discordant and fall on, or to the right of, the dike data, indicating crystallization at ~3.1 Ga. The results indicate that a kilometer-thick body of 3.1 Ga tonalite gneiss lies within the lower crustal complex, and mapping indicates that lenses of such tonalite gneiss are widespread in the lower part of the section.

At Site B, a meter-thick dike of granite pegmatite that cross-cuts felsic charnockite gneiss of the lower crustal domain was sampled 100 m south of a fault contact with the middle crustal granites (Fig. 2). Three zircon grains yield a linear array of slightly discordant results, consistent with impact-related alteration and Pb-loss (Table 1). Regression of data through the age of the impact event yields an upper intercept with concordia of 3.094 ± 0.007 Ga (mean square weighted deviance = 1.5) (*19*), the interpreted crystallization age. This granite dike, which is undeformed along strike for tens of meters, falls within the range of Pb-Pb, and Th-Pb whole rock isochron ages obtained for the nearby middle crustal granites (*15*). It is further evidence of an intrusive relation between the middle and lower crust and is a lower limit on the age range of deep crust lithologies.

Mapping and U-Pb dating evidence indicate that the middle and lower crust of the Vredefort crustal cross section were created and/or assembled during a major, dynamic event at 3.11 ± 0.01 Ga. The dynamic nature of this event is evident from the metamorphic age of sedimentary rocks in the lower crustal domain (garnet-bearing paragneiss, Fig. 2). These clastic units, interlayered with units of metamorphosed banded iron formation (*14*), yield primary Th-Pb and Sm-Nd ages of ~3.5 Ga (*15*) but were not metamorphosed in the lower crust until 3.11 ± 0.01 Ga (*16*). The occurrence of these originally supracrustal rocks in a granulite-facies metaplutonic domain indicates transport to depth during this event. The xenolith suite of the Jurassic Lace kimberlite pipe, 70 km to the southwest of the study area, contains an abundance of Archean, lower crustal, sapphirine-bearing granulites (ultrametamorphosed clastic sediments) (*20*), suggesting that thrusting of sedimentary rocks to the lower crust was regionally significant. This is difficult to reconcile with the presence at this time of a stable 3.2 Ga mantle root.

The 3.11 ± 0.01 Ga underthrusting and reworking of 3.5 Ga crust was followed closely by intrusion of tonalitic, granitic, and syenitic magmas at least as young as 3.092 ± 0.007 Ga to form the ~10-km-thick middle crust and perhaps 20% of the lower crust. The upper crustal manifestation of this event is the emplacement of kilometer-scale bodies of syenite and granite across the craton (*1*) and transcurrent shearing along pre-existing faults (*7*). The abundance of incompatible elements and xenocrystic zircon in these late, pan-cratonic granitoid intrusions (*15*, *21*) suggests derivation by partial melting of Mesoarchean crust. On the basis of the distribution of rock types in the Vredefort crustal cross section, as much as 40% of the crust may have been re-melted during the 3.11 Ga event. The intensity of the thermal event responsible for this degree of crustal melting is, again, inconsistent with the persistence of a stable mantle root beneath the crust during this time.

Faced with the evidence for remobilization of the deep Kaapvaal lithosphere between 3.11 ± 0.01 Ga and 3.094 ± 0.007 Ga, the question arises as to the cause. Thickening of the crust at a collisional plate margin could account for the history of sediment underthrusting and magmatism; however, there is no evidence in the structural and metamorphic record of the upper crust of the craton for orogeny at 3.11 Ga. Complete delamination of pre-existing mantle lithosphere and replacement by hotter asthenosphere would provide a heat source for lower crustal melting but fails to account for the persistence of old (3.5 to 3.2 Ga) peridotites identified in the present mantle root (*2*). A plausible alternative is that partial delamination of mantle lithosphere occurred during a period of 3.1 Ga oceanic-continental plate convergence, producing a mantle root melange of subduction and presubduction origin. Accompanying vertical lithospheric strain did not propagate into the upper crust; instead, it was accomodated by deep crustal ductile flow in a hotter Archean crust (e.g., *22*, *23*). Regardless, the identification of 3.11 ± 0.01 Ga remobilization of deep lithosphere after assembly of 3.5 to 3.2 Ga crustal and mantle components indicates a period of

Table 1. U-Pb data. Unless otherwise stated all the zircons are clear, transparent grains from least paramagnetic fractions of Frantz separates and are free of cracks and inclusions. [s], single-grain fraction. U concentrations are known to better than 5% for sample weights over 50 μg and about 50% for sample weights below 2 μg. Pb_{com}, total common Pb (corrected for fractionation and spike). A run-dependent laboratory blank, ranging from 1 to 2 pg, was subtracted from total Pb. The remainder was considered "inherited" Pb (in some cases on impact fractures), the composition of which was estimated using a model (*30*) where t = 3100 million years ago (Ma). Model Th/U was inferred from $^{208}Pb/^{206}Pb$ using the $^{207}Pb/^{206}Pb$ age (i.e., a minimum estimate). The ratio of $^{206}Pb/^{204}Pb$ was corrected for fractionation and spike. All other Pb ratios here were corrected for fractionation, spike, blank Pb, and initial common Pb if total common Pb > 2 pg for single grains. Uncertainty was estimated with error propagation procedure that accounts for measurement errors, blank uncertainties, reproducibility of Pb and U standards, and the effect of an uncertainty of ±2% on the initial Pb composition and 1% on the blank Pb composition. Uncertainties on ratios and ages are quoted at the 2σ level of confidence. % disc, percent discordance. Error values for the final digits of the isotopic ratios are given in parentheses.

Fraction no.	Weight (μg)	U (ppm)	Pb_{com} (pg)	Th/U	$^{206}Pb/^{204}Pb$	$^{206}Pb/^{238}U$	$^{207}Pb/^{235}U$	$^{207}Pb/^{206}Pb$	$^{207}Pb/^{206}Pb$ (Ma) [% disc]
Site A: Foliated tonalite dyke									
Z3 [s]	4	150	1.3	0.5	16,994	0.5815 (20)	18.237 (64)	0.22748 (28)	3034 ± 2 [3.3]
Z5 [s]	1	370	1.6	0.2	8,450	0.5854 (22)	18.335 (70)	0.22717 (20)	3032 ± 3 [2.5]
Z4 [s]	2	425	4.1	0.2	7,279	0.5472 (22)	16.212 (60)	0.21488 (46)	2943 ± 3 [5.4]
Z8 [s]	8	210	0.8	0.9	7,843	0.6038 (20)	19.361 (70)	0.23258 (28)	3070 ± 2 [1.0]
Site A: Tonalite gneiss									
Z1 [s]	2	115	1.7	0.4	4,803	0.5437 (21)	13.043 (66)	0.21401 (28)	2936 ± 2 [5.8]
Z3 [s]	3	100	2.8	1.3	4,092	0.5755 (20)	17.848 (62)	0.22491 (30)	3016 ± 2 [3.5]
Z4 [s]	1	130	0.8	0.8	6,288	0.5709 (16)	17.492 (54)	0.22223 (24)	2997 ± 2 [3.5]
Site B: Granite dyke									
Z2 [s]	1	25	0.7	1.0	1,413	0.5876 (120)	18.40 (40)	0.2271 (12)	3032 ± 8 [2.1]
Z4 [s]	7	60	7.4	0.9	2,140	0.5871 (20)	18.461 (72)	0.22805 (34)	3038 ± 2 [2.5]
Z5 [s]	12	70	2.9	0.6	11,160	0.5911 (82)	18.73 (26)	0.22985 (46)	3051 ± 3 [2.3]

decoupling between the Kaapvaal crust and its present mantle root. It follows that Archean crust can couple to Archean mantle at more than one time before the birth of the tectosphere.

Our data place a maximum age of 3.09 Ga on the time of crust-root coupling, given that this is the last recognized time of voluminous granite magmatism in the Vredefort section. Magmatic intraplating and/or impact related effects at the crust-mantle boundary have caused local granulite-facies metamorphism at 2.7, 2.0, and 1.0 Ga (*24*, *25*), but these thermal events in the Mesoarchean crust as a whole have been minor relative to the events at ~3.1 Ga. The presence of Neoarchean dolerite dykes (*16*) also argues against elevated (>400°C) crustal temperatures after this time. A lower limit of 3.07 Ga for tectosphere birth is derived from the age of basal volcanic and sedimentary rocks of the Witwatersrand Basin, part of a passive continental margin sequence deposited on the stabilized crystalline crust (*1*, *7*). On the basis of these upper and lower age limits, we place the age of permanent crust-mantle coupling (tectosphere initiation) beneath the central Kaapvaal crust at 3.08 ± 0.01 Ga.

Given our 3.08 Ga age for Kaapvaal tectosphere birth, there is a ~120 million year gap between the 3.2 Ga assembly of the Mesoarchean crust of the craton (*7*) and its coupling to the mantle root. This indicates an allocthonous relation between the crust and mantle root, consistent with continental genesis models that portray crust and mantle lithosphere as components generated in different tectonic settings before unification (e.g., *3*, *5*). A model of root formation by accretion of oceanic lithosphere plates (*5*) is supported by recent Re-Os dating that reports about 3 Ga eclogitized oceanic crust beneath much of the craton (*26*). Moreover, the discovery of 2.86 ± 0.06 Ga sulphide inclusions in eclogitic diamonds beneath the center of the craton indicates root thickening to >150 km (the approximate depth to diamond stability field) by this time (*27*). Thus, the construction of the tectosphere took place within roughly 0.2 Gy of tectosphere initiation.

Our integrated mapping and high-precision geochronology of the deep Kaapvaal crust demonstrates that tectosphere birth can post-date the age of its crust and mantle components by several hundred million years, with crust assembly preceding subduction-driven mantle root construction by at least 0.12 Ga. A similar rate and process of tectosphere genesis later in the Archean can be inferred from limited data for 2 of the 10 other tectosphere fragments; namely the Superior craton of North America (*22*, *28*) and the Siberian craton (*29*). Further lower crust and mantle root geochronology will test whether indeed all such ancient continental plates were created equally.

References and Notes

1. G. Brandl, M. J. de Wit, in *Greenstone Belts*, M. J. de Wit, L. D. Ashwal, Eds. (Oxford Monographs on Geology and Geophysics, Oxford, UK, 1997), vol. 35, chap. 5.8, pp. 581–607.
2. R. W. Carlson *et al.*, in *Proceedings of the 7th International Kimberlite Conference*, J. J. Gurney, J. L. Gurney, M. D. Pascoe, S. H. Richardson, Eds. (Red Roof Design, Cape Town, 1999), pp. 99–108.
3. T. H. Jordan, *Rev. Geophys. Space Phys.* **13**, 1 (1975).
4. F. R. Boyd, *Earth Planet. Sci. Lett.* **96**, 15 (1989).
5. H. Helmstaedt, D. J. Schulze, *Geol. Soc. Aust.* **14**, 358 (1989).
6. S. H. Richardson, J. J. Gurney, A. J. Erlank, J. W. Harris, *Nature* **310**, 198 (1984).
7. M. J. de Wit *et al.*, *Nature* **357**, 553 (1992).
8. R. J. Hart, M. A. G. Andreoli, M. Tredoux, M. J. de Wit, *Chem. Geol.* **82**, 21 (1990).
9. A. A. Nyblade, in *Composition, Deep Structure and Evolution of Continents*, R. D. van der Hilst, W. F. McDonough, Eds., *Lithos* **48** (Scientific Publishers, Amsterdam, 1999), pp. 81–91.
10. M. Tredoux, R. J. Hart, R. W. Carlson, S. B. Shirey, *Geology* **27**, 923 (1999).
11. D. E. Moser, *Geology* **25**, 7 (1997).
12. A. M. Therriault, R. A. F. Grieve, W. U. Reimold, *Meteoritics* **32**, 71 (1997).
13. R. L. Gibson, G. Stevens, *Geol. Soc. London Spec. Publ. 138* (1998), pp. 121–135.
14. D. Stepto, *Tectonophysics* **171**, 75 (1990).
15. R. J. Hart, H. J. Welke, L. O. Nicolaysen, *J. Geophys. Res.* **86**, 10663 (1981).
16. R. J. Hart, D. E. Moser, M. Andreoli, *Geology* **27**, 1091 (1999).
17. R. M. Flowers, thesis, University of Utah (2000).
18. D. W. Davis, *Can. J. Earth Sci.* **11**, 2141 (1982).
19. K. R. Ludwig, U.S. Geol. Surv. Open-File Rep. 91-0445, (1991).
20. J. B. Dawson, S. L. Harley, R. L. Rudnick, T. R. Ireland, *J. Metamorph. Geol.* **15**, 253 (1997).
21. L. J. Robb, D. W. Davis, S. L. Kamo, F. M. Meyer, *Nature* **357**, 677 (1992).
22. D. E. Moser, L. M. Heaman, T. E. Krogh, J. A. Hanes, *Tectonics* **15**, 1093 (1996).
23. L. Royden, *J. Geophys. Res.* **101**, 17679 (1996).
24. D. E. Moser, R. J. Hart, in *Proceedings of the 7th International Kimberlite Conference*, Cape Town, 13 to 17 April 1998 (Univ. of Cape Town, Cape Town, 1998), pp. 609–611.
25. M. Schmitz, S. Bowring, *Chem. Geol.*, **172**, 59 (2001).
26. S. B. Shirey *et al.*, *Geophys. Res. Lett.*, in press.
27. S. H. Richardson, S. B. Shirey, J. W. Harris, R. W. Carlson, in preparation.
28. D. G. Pearson, H. O. A. Meyer, F. R. Boyd, S. B. Shirey, R. W. Carlson, in *Proceedings of the 6th International Kimberlite Conference*, Novosibirsk, 7 to 13 August 1995 (Russian Academy of Science, Siberia, 1995), pp. 427–429.
29. D. Jacob, E. Jagoutz, D. Lowry, D. Mattey, G. Kudrjavtseva, *Geochim. Cosmochim. Acta* **58**, 5191 (1994).
30. J. S. Stacey and J. D. Kramers, *Earth Planet. Sci. Lett.* **26**, 207 (1975).

31. Supported by NSF grant no. EAR9805210. Resources for U-Pb dating (Royal Ontario Museum) and initial logistical support from M.J. de Wit (University of Cape Town) are gratefully acknowledged, as are discussions with our U.S. and African collegues in the Kaapvaal Craton Project.

12 October 2000; accepted 4 December 2000

Sound Velocities in Iron to 110 Gigapascals

Guillaume Fiquet,[1]* James Badro,[1] François Guyot,[1] Herwig Requardt,[2] Michael Krisch[2]

The dispersion of longitudinal acoustic phonons was measured by inelastic x-ray scattering in the hexagonal closed-packed (hcp) structure of iron from 19 to 110 gigapascals. Phonon dispersion curves were recorded on polycrystalline iron compressed in a diamond anvil cell, revealing an increase of the longitudinal wave velocity (V_P) from 7000 to 8800 meters per second. We show that hcp iron follows a Birch law for V_P, which is used to extrapolate velocities to inner core conditions. Extrapolated longitudinal acoustic wave velocities compared with seismic data suggest an inner core that is 4 to 5% lighter than hcp iron.

The knowledge of the elastic constants of the phases of iron, which makes up 70 to 90 weight % of planetary cores, is essential for comparison with global velocity models of Earth. The hcp (or ε) high-pressure phase of iron is stable to at least 300 GPa at ambient temperature (*1*). Elastic properties of hcp iron have been determined to 210 GPa by x-ray diffraction (XRD) lattice strains measurements (*2*, *3*), but these results show discrepancies with calculations using first-principles methods (*4-7*), as well as with a recent experimental investigation to 42 GPa by nuclear resonant inelastic x-ray scattering (NRIXS) of synchrotron radiation (*8*). The most recent investigation with NRIXS (*9*), however, yielded results consistent with lattice strain measurements (*3*). Elastic properties of hcp iron determined by Raman spectroscopy to 156 GPa yielded a C_{44} elastic modulus that is lower than previous determinations (*10*). Inconsistencies among these studies might be partly attributed to the fact that none of these techniques directly measures the acoustic wave velocities of iron. This limitation can be overcome by inelastic x-ray scattering (IXS) with meV energy resolution, where the acoustic velocity can be directly derived from the dispersion of the acoustic phonon energy (*11*, *12*).

Our IXS experiment was carried out at the inelastic scattering beamline ID28 at the European Synchrotron Radiation Facility

[1]Laboratoire de Minéralogie et Cristallographie, UMR CNRS 7590, Université Paris VI, 4 Place Jussieu, 75252 Paris cedex 06, France. [2]European Synchrotron Radiation Facility, BP220, 38043 Grenoble cedex, France.

*To whom correspondence should be addressed. E-mail: fiquet@lmcp.jussieu.fr